https://doi.org/10.1038/s44407-026-00080-7

Large inter-model spread in simulated aerosol load over Arctic sea ice

Basudev Swain[1] ✉, Marco Vountas[2] ✉, Aishwarya Singh[3], Linus Andrae[2], Ina Tegen[4], Luca Lelli[5], Rui Song[6], Bernd Heinold[4], Neha Mehendale[2] & Hartmut Bösch[2]

Before the development of AEROSNOW aerosol optical depth (AOD) retrievals over Arctic sea ice, comprehensive observations across the central sea-ice region were limited, and understanding of aerosol variability relied largely on models. We evaluate how sixteen CMIP6 models simulate AOD over Arctic sea ice using AEROSNOW observations, focusing on spring Arctic Haze and summer clean-air conditions. Observations show localized spring AOD maxima (0.12–0.18) near marginal ice zones adjacent to northern Canada, Alaska, and Siberia, followed by a decline to 0.05–0.07 in summer. Most models (12 of 16) underestimate the spring enhancement by 40–75%, while four overestimate it by up to 340%, reflecting differences in aerosol composition, transport, and wet scavenging. Although the multi-model mean approximates observations due to compensating biases, IPSL-CM5A2-INCA, EC-Earth3-AerChem, and MRI-ESM2-0 produce seasonal mean AOD values closer to AEROSNOW. Among them, EC-Earth3-AerChem captures the observed seasonal amplitude and monthly variability more consistently.

The Arctic is experiencing enhanced warming relative to the global mean, a phenomenon widely referred to as Arctic Amplification (AA)[1]. This accelerated warming affects the entire Arctic region and is primarily driven by increasing concentrations of anthropogenic greenhouse gases and associated climate feedbacks[2,3]. In addition to these dominant drivers, aerosols influence the regional energy balance by modifying solar radiation through scattering and absorption and by altering cloud microphysical properties and radiative forcing through their role as cloud condensation nuclei and ice-nucleating particles[4]. Although aerosols are not considered a primary cause of Arctic Amplification, their interactions with radiation and clouds can modulate surface energy fluxes and contribute to regional climate variability.

The spring and summer seasons strongly influence seasonal variations in aerosol distribution over the Arctic. In spring (March–May), poleward transport of pollutants from the lower latitudes introduces large amounts of dust and sulfate aerosols, giving rise to the well-known "Arctic Haze"[5–7]. In contrast, the summer period (June–August) is characterized by a dominance of locally produced natural aerosols, efficient wet scavenging through precipitation, and overall low particle concentrations, conditions often referred to as the "clean-Arctic" state[5,6,8–10]. These pronounced seasonal cycles influence radiative fluxes, cloud formation, and large-scale atmospheric circulation patterns[11,12]. Although AOD values over Arctic sea ice are relatively low, even small variations in aerosol loading can lead to significant changes in radiative forcing and cloud properties in this highly sensitive environment, thereby influencing surface energy balance and contributing to uncertainties in Arctic climate projections[11,12]. Despite their importance, our current understanding of aerosol seasonality and its climatic implications over Arctic sea-ice remains largely based on model simulations, as long-term and spatially and temporally extensive observations from ground-based and satellites are still lacking.

Several dedicated field campaigns have contributed valuable in situ aerosol datasets[13–16]. However, their coverage is limited both spatially and temporally, thus large regions of the central Arctic sea-ice region are poorly characterized. The satellite observations could, in principle, fill this observational gap by providing spatially continuous aerosol load distributions. Yet, remote sensing of aerosols over snow- and ice-covered surfaces of the sea-ice region is challenging because of strong surface reflectance and persistent cloudiness[7,8,17,18]. These factors introduce significant uncertainty into satellite retrievals and limit their reliability across much of the Arctic sea-ice domain[18]. Various retrieval algorithms have been proposed to mitigate these issues using top-of-atmosphere reflectance data[19–22], though most efforts

[1]Department of Physics, Atmospheric, Oceanic and Planetary Physics, University of Oxford, Oxford, UK. [2]Institute of Environmental Physics, University of Bremen, Bremen, Germany. [3]Aerosol Chemistry Department, Max-Planck Institute for Chemistry, Mainz, Germany. [4]Department Modelling of Atmospheric Processes, Leibniz Institute for Tropospheric Research, Leipzig, Germany. [5]Remote Sensing Technology Institute, German Aerospace Centre (DLR), Wessling, Germany. [6]NCEO, Department of Physics, Atmospheric, Oceanic and Planetary Physics, University of Oxford, Oxford, UK. ✉e-mail: basudev.swain@physics.ox.ac.uk; vountas@iup.physik.uni-bremen.de

have focused on specific sub-regions such as Svalbard island, leaving vast sea-ice-covered areas underrepresented.

In the absence of high spatial and temporal observational coverage from satellites, atmospheric reanalysis datasets[18,23,24] are commonly employed as proxies for direct measurements to study aerosol variability and its climatic impact over the Arctic. However, these reanalyses ultimately depend on model-based simulations and are not well constrained by actual observations across the sea-ice domain. As a result, significant uncertainties persist regarding their representation of Arctic aerosol load and its processes.

To improve observational constraints, the AEROSNOW retrieval framework was recently designed to retrieve aerosol optical depth (AOD) more accurately over sea-ice regions of the Arctic[25]. By considering the bidirectional reflectance distribution function (BRDF) parameterizations[26] and improved cloud screening[27]. Thus, AEROSNOW provides high-resolution spatio-temporal observations of aerosol load across the Arctic sea-ice domain for the period 2003–2011, covering nearly a decade. It also offers an opportunity to evaluate the performance of various numerical models in simulating Arctic Haze and Clean-Air regimes over sea-ice regions.

In this study, we combine AEROSNOW satellite observations with simulations from sixteen atmospheric numerical models to evaluate how well current models reproduce the observed seasonal patterns of aerosol loading over Arctic sea ice. Our analysis reveals substantial discrepancies between model outputs and AEROSNOW observations, suggesting that existing numerical models are far from estimating the spring and summer evolution of aerosols over this region. These results underscore the importance of advancing model parameterizations and the observational constraints to more accurately represent aerosol seasonality and its subsequent impact on regional climate and the Arctic warming over the Arctic sea-ice domain.

Results

Models fail to simulate seasonal air pollution spatial patterns over the arctic sea-ice

The seasonal variability of AOD over Arctic sea-ice-covered regions shows a clear spatial distribution contrast of AOD between spring and summer (Fig. 1). AEROSNOW retrievals indicate that during spring (April–May), area-averaged AOD over the entire sea-ice reaches approximately 0.08 ± 0.01, with localized maximum AOD of 0.12-0.18 occurring near marginal ice zones in the Eurasian and North Atlantic sectors. These enhanced values are consistent with the Arctic Haze period[5,6], which is associated with long-range transport of sulfate- and black-carbon-rich aerosols from mid-latitude source regions. In summer (June–August), area-averaged AOD decreases to about 0.05-0.07 over the entire sea-ice domain, with lower spatial AOD variability compared to spring. This seasonal reduction is consistent with increased wet scavenging and weaker meridional transport of anthropogenic aerosols[6,28]. Natural marine and biogenic sources dominate during this period, contributing to cleaner atmospheric conditions and a reduction in column aerosol loading[6,11,28]. This indicates that AEROSNOW observes both the seasonal changes in Arctic Haze and clean-air conditions across sea-ice areas of the Arctic.

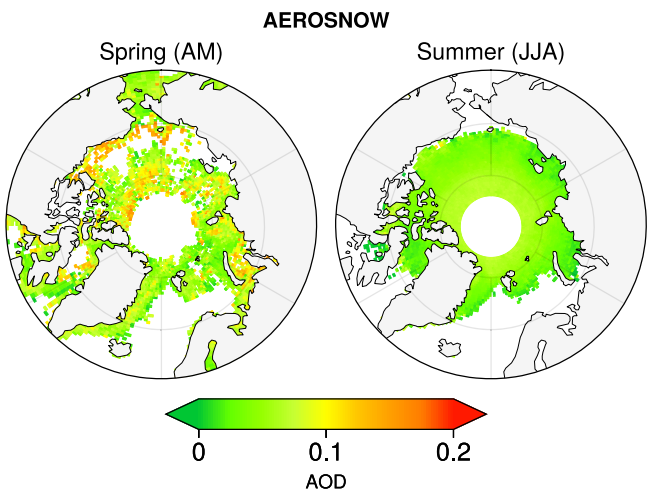

Fig. 1 | Average spring and summer AOD over the central Arctic sea-ice region (2003–2011) retrieved using the AEROSNOW algorithm. Mean aerosol optical depth (AOD) for spring (April–May) and summer (June–August) derived from AATSR observations with the AEROSNOW retrieval[25].

Model-simulated AODs from sixteen different models exhibit substantial variability in both magnitude and aerosol load across sea-ice in relation to AEROSNOW retrievals (Fig. 2a–p). Although most of the models qualitatively reproduce the lower AOD values observed in summer relative to spring, they fail to capture the full amplitude of this seasonal transition. Several models—including MIROC6, CNRM-ESM2-1, IPSL-CM6A-LR, CESM2-WACCM-FV2, MPI-ESM-1-2-HAM, NorESM2-LM, NorESM2-MM, IPSL-CM6A-LR-INCA, IPSL-CM5A2-INCA, EC-Earth3-AerChem, and MRI-ESM2-0 simulate springtime mean AODs of only 0.04-0.07 (Fig. 2a–k), underestimating retrieved values by approximately 50 to 75%. Among these, EC-Earth3-AerChem and MRI-ESM2-0 show the smallest biases, with underestimations below—25% (Fig. 3a–c). In contrast, models such as GISS-E2-1-G, GISS-E2-1-H, INM-CM5-0, INM-CM4-8, and GISS-E2-2-G produce unrealistically high spring AODs exceeding 0.25 (Fig. 2l-p), overestimating observed levels by 150–340% (Fig. 3a-c). These inconsistencies likely stem from differences in model representations of aerosol emissions, microphysics, and transport processes, as well as removal mechanisms[6,7,11,18]. Underestimation may result from coarse-resolution transport schemes that constrain poleward aerosol advection[7,18], whereas overestimation could stem from inadequate wet deposition parameterizations or overly efficient secondary aerosol formation in cold, stable boundary layers[11,12]. The systematic differences between AEROSNOW and models become more apparent when expressed as relative percentage deviations from AEROSNOW data (Fig. 3a-c). Across the ensemble, 11 out of 16 models underestimate spring AOD by more than 50%, with several exceeding 75% negative bias, while the remaining models overestimate AOD by 150% to 340% (Fig. 3a). During summer, underestimation persists for most models, though the bias magnitude tends to decrease, likely because cleaner background conditions reduce sensitivity to emission and removal parameterizations (Fig. 3b). Nevertheless, some models invert the bias sign in summer, indicating an overcompensation of naturally occurring aerosol types, particularly, sea-salt and biogenic aerosols. Overall, the ensemble-mean bias remains negative across both seasons, confirming that CMIP6 models systematically fail to reproduce both the magnitude and seasonality of Arctic aerosol loading (Fig. 3a–c).

These biases have important implications for Arctic climate representation. Underestimated aerosol concentrations lead to lower simulated atmospheric absorption and weaker shortwave dimming, potentially enhancing local radiative warming and contributing to sea-ice melt biases[14]. Conversely, models that overestimate AOD may exaggerate aerosol-cloud interactions, producing unrealistic cooling and altered cloud microphysical properties[14,29]. The observed inability of current numerical models to capture the true seasonal amplitude of AOD variability indicates that multiple processes are likely contributing to these biases. In addition to aerosol transport and removal processes, particularly wet scavenging, dry deposition, and vertical mixing, differences in the representation of aerosol and precursor emissions may also play an important role over the Arctic sea-ice domain[6,11,12,29].

Models simulated monthly mean temporal changes are far from satellite observations

The seasonal variability of AOD over Arctic sea-ice-covered regions (≥72°N) shows a modest spring-summer contrast (Fig. 1). AEROSNOW retrievals indicate that in spring (April–May), the area-averaged AOD reaches 0.08 ± 0.01, with localized maxima (0.12–0.18) near marginal ice zones bordering northern Canada, Alaska, and Siberia, consistent with the

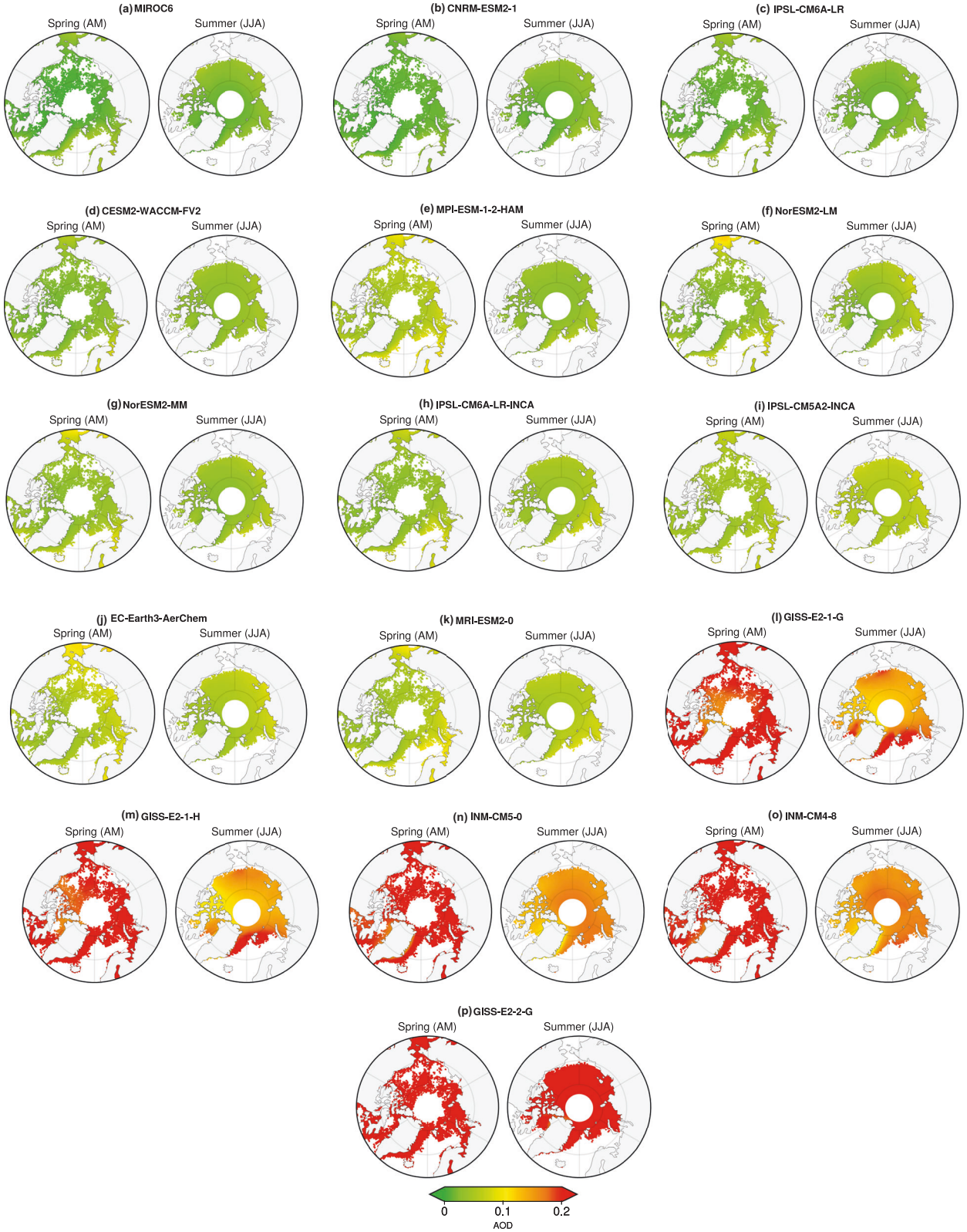

Fig. 2 | Seasonal mean AOD simulated by CMIP6 models (2003-2011) over the Arctic sea-ice region. a–p show spring (April–May) and summer (June–August) mean total aerosol optical depth (AOD) simulated by different CMIP6 models for areas corresponding to AEROSNOW observations. **a–k** represent models with relatively low AOD, whereas **l–p** represent models with higher AOD values.

Arctic haze period. In summer (June–August), AOD decreases to 0.05–0.07 across the same region, with weaker spatial variability. This seasonal transition is consistent with enhanced wet scavenging and weaker meridional transport of anthropogenic aerosols[6]. This pattern reflects the classical Arctic Haze phenomenon—dominated by long-range transport of anthropogenic sulfate and black carbon during spring—and a transition to cleaner summer conditions characterized by enhanced wet scavenging and weaker transport from mid-latitudes[6].

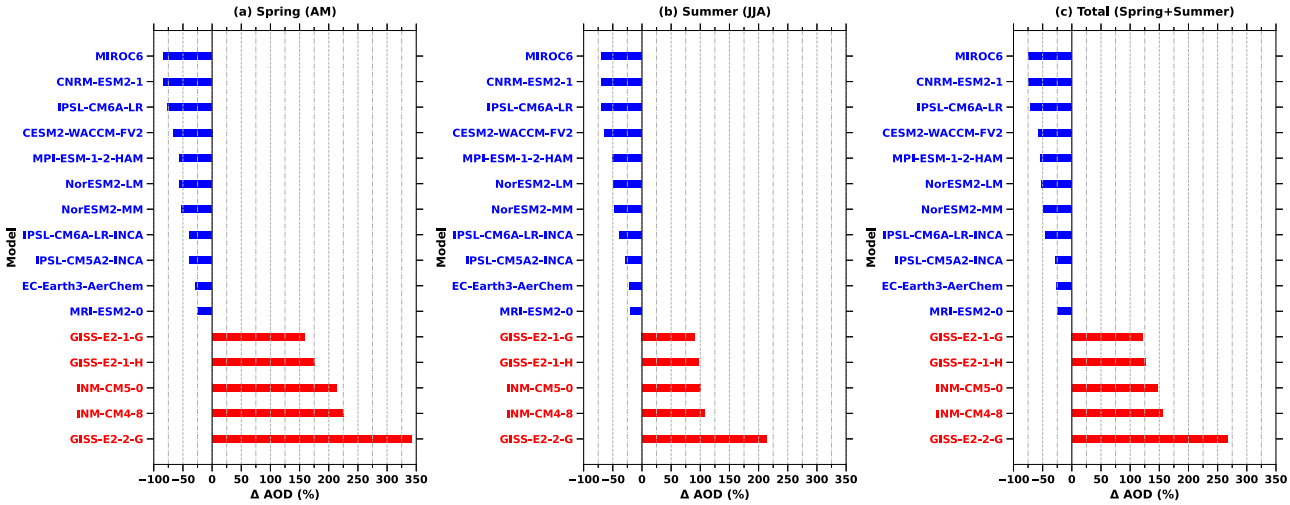

Fig. 3 | Relative bias in AOD simulated by CMIP6 models compared to AEROSNOW observations over Arctic sea ice. a–c show the percentage differences in mean AOD during spring (April–May), summer (June–August), and the combined period (spring + summer). Models are ranked along the y-axis, with blue and red bars indicating underestimation and overestimation relative to AEROSNOW measurements, respectively.

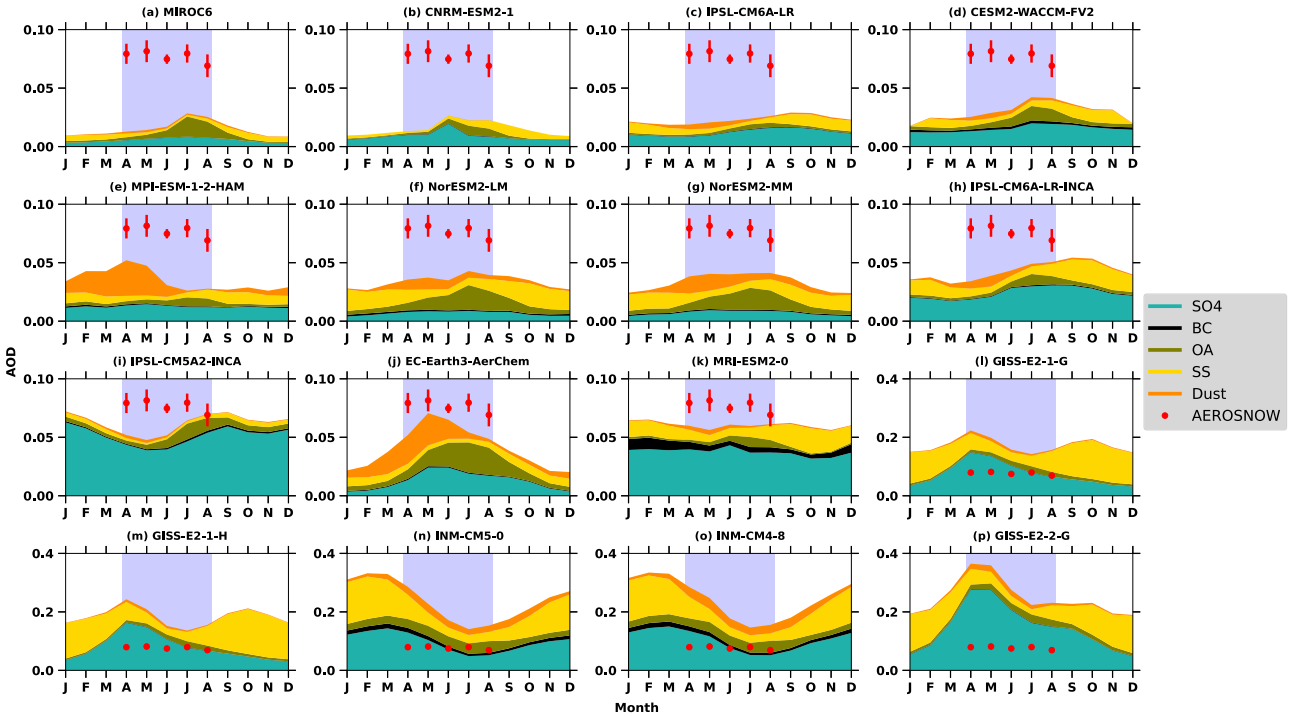

Fig. 4 | Monthly-mean seasonal AOD and composition over Arctic sea ice, averaged across the years 2003–2011 model simulations. Sections with a blue background show the Spring and Summer seasons with corresponding AEROSNOW measurements depicted in red. Total AOD is separated into SO_4, BC, OA, SS, and Dust components for each model. The low-AOD and high-AOD models' Y-axis values are 0.10 and 0.40, respectively.

In contrast, the CMIP6 simulations exhibit systematic biases in both the magnitude and timing of monthly mean AOD relative to AEROSNOW (Fig. 4a–p). Several models (MIROC6, CNRM-ESM2-1, IPSL-CM6A-LR, CESM2-WACCM-FV2, MPI-ESM-1-2-HAM, NorESM2-LM, NorESM2-MM, IPSL-CM6A-LR-INCA, IPSL-CM5A2-INCA, and MRI-ESM2-0) simulate monthly mean AOD values that are consistently lower than observed, typically around 0.04–0.05 throughout the analyzed period. Conversely, GISS-E2-1-G, GISS-E2-1-H, INM-CM5-0, INM-CM4-8, and GISS-E2-2-G produce substantially higher AOD values (up to 0.25–0.38, overestimating by 200–300%), resulting in persistent positive biases. The multi-model mean (MMM) peaks near 0.11 in April, slightly exceeding the observed spring mean and reproducing the general spring-to-summer decrease; however, this agreement arises from compensating high and low biases across models rather than consistent representation of the observed spring and summer evolution (Fig. 5).

The additional zonal AOD and precipitation diagnostics presented in Fig. 6 show that while the seasonal structure of precipitation is broadly similar across models, its magnitude and intensity differ. These differences in precipitation intensity coincide with variations in simulated AOD levels among individual models. In particular, EC-Earth3-AerChem[30] exhibits a springtime AOD enhancement at high latitudes, followed by a summer reduction that coincides with increased precipitation intensity (Fig. 6). It is worth noting that the EC-Earth3-AerChem model[30] (Fig. 4j) distinguishes itself from the other models (Fig. 4) through its advanced and physically

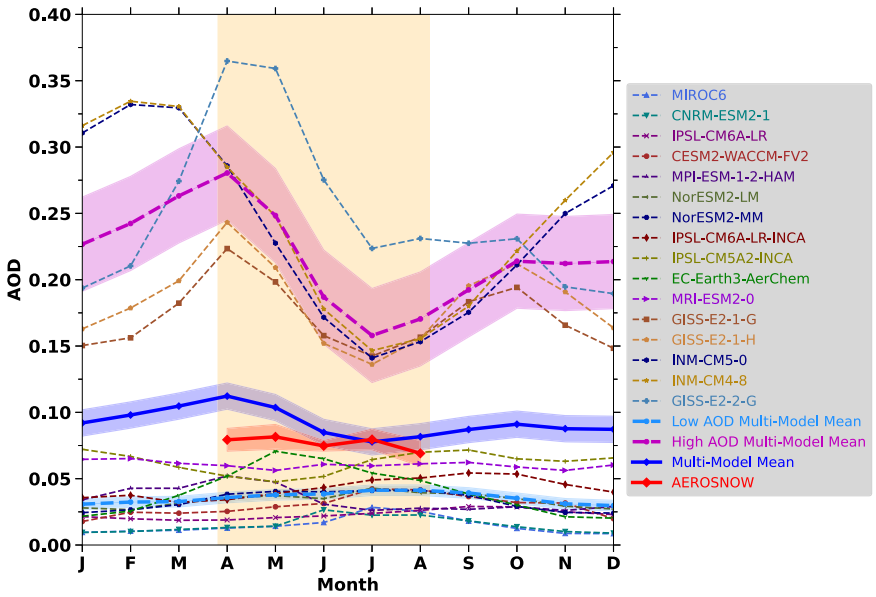

Fig. 5 | Monthly-mean seasonal AOD and composition over Arctic sea ice, averaged across the years 2003–2011 model simulations. The total AOD simulated by each model over Arctic sea-ice for each month. The multi-model mean of high-AOD simulating models and low-AOD simulating models, as well as the mean of all the models,are presented with AEROSNOW retrievals.

consistent parameterizations of both atmospheric chemistry and meteorology during its participation in CMIP6. EC-Earth3-AerChem was parameterized according to the framework described by ref. 30 for its participation in CMIP6, incorporating comprehensive representations of aerosol processes and atmospheric dynamics that yield a more realistic simulation of aerosol seasonality over the Arctic. Unlike models that rely on simplified or prescribed aerosol fields, EC-Earth3-AerChem features interactive aerosol microphysics, detailed gas-phase and heterogeneous chemistry, and dynamically coupled aerosol-cloud-radiation interactions[30]. In particular, its explicit treatment of wet scavenging—including cloud-phase-dependent removal and precipitation-driven processes—enhances the simulation of aerosol lifetimes and seasonal variability[30]. The well-resolved meteorological fields, combined with an improved depiction of transport and mixing, enable the model to accurately reproduce the observed transition from high springtime Arctic haze to the cleaner summertime atmosphere over the Arctic sea-ice domain.

Owing to this tight coupling between chemistry, aerosol processes, and meteorology, EC-Earth3-AerChem exhibits smaller AOD biases and a closer representation of the amplitude of the monthly aerosol cycle compared with many other numerical models used in CMIP6 (Figs. 4 and 6), underscoring the benefits of its comprehensive physical and chemical parameterizations for simulating Arctic aerosol-climate interactions. Although the comparison of individual models presented in Fig. 6 does not establish direct causality, it suggests that differences in removal strength may contribute to the inter-model spread in AOD (Figs. 4 and 6).

Models that simulate lower total AOD generally also produce lower sulfate and dust contributions, while models with higher total AOD tend to simulate enhanced sulfate and sea-salt fractions, particularly during summer. These inter-model differences in species partitioning contribute to differences in the simulated monthly evolution of total AOD (Fig. 5). However, because individual aerosol components are not directly constrained by the satellite retrievals, these comparisons should be interpreted as structural differences among models rather than as validated compositional estimates. When grouped by their overall AOD bias, the low-AOD models maintain persistently lower aerosol burdens throughout the analyzed period, whereas the high-AOD models simulate consistently elevated values. These differences likely reflect variations in the representation of emissions, transport, and removal processes across models, although process-level diagnostics were not explicitly evaluated here. Consequently, the multi-model mean lies between these extremes but does not fully capture the observed monthly evolution of total AOD. Overall, the CMIP6 ensemble exhibits substantial spread in both the magnitude and seasonal progression of simulated AOD over Arctic sea-ice-covered regions (Figs. 3 and 4). These differences underscore the sensitivity of Arctic aerosol simulations to model-specific representations of aerosol life-cycle processes and highlight the need for further process-oriented evaluation.

Identification of models suitable for arctic aerosol variability studies

This section identifies models that are comparatively suitable for studying aerosol variability over Arctic sea-ice-covered regions based on their agreement with AEROSNOW observations. Model performance is evaluated using seasonal mean AOD, monthly evolution, and seasonal amplitude. Evaluation of the seasonal mean AOD and its compositional components across CMIP6 models reveals substantial inter-model variability over Arctic sea-ice-covered regions. For spring (April–May) (Fig. 7a–f). This value represents the spatial mean across all sea-ice-covered grid cells and should be distinguished from localized maxima near marginal ice zones shown in Fig. 1. The elevated spring mean is consistent with enhanced aerosol loading during the Arctic Haze period, driven primarily by long-range transport of anthropogenic sulfate and black carbon into the high Arctic. Model-simulated AOD values, however, range widely from 0.04 to 0.07 in the underestimating models to 0.25–0.40 in the overestimating models, reflecting differences exceeding a factor of five between extremes (Fig. 7a–f). Similar patterns persist during summer (June–August), although overall AOD levels decline slightly due to reduced anthropogenic transport and increased wet scavenging. The MMM reproduces a total AOD close to the AEROSNOW observations, yet this apparent agreement masks large and opposing biases across individual models (Fig. 7a–c).

Decomposition of AOD into its constituent species highlights the sources of these biases (Fig. 7d–f). In most models, sulfate (SO_4) dominates total aerosol loading, accounting for 45–70% of AOD, followed by sea-salt (SS) and organic aerosols (OA), contributing 20–30% and 10–15%, respectively. The low-AOD models simulate unrealistically low SO_4 and black carbon (BC) levels, implying excessive scavenging and weak long-range transport from mid-latitudes. In contrast, high-AOD models exaggerate SO_4 and SS burdens, sometimes exceeding 0.30–0.35 AOD, indicating overactive marine emissions or inefficient removal. These divergent behaviors produce an MMM that lies between extremes but does not represent a physically consistent aerosol regime (Fig. 7d–f).

The percentage deviation of individual aerosol components from the MMM further emphasizes this imbalance (Fig. S1). During spring, SO_4 and BC differ by more than ±150% across models, with the low-AOD models systematically underpredicting, and those with high AOD consistently overpredicting relative to the mean. In summer, similar divergence occurs for SS and OA, where some models overpredict by 200–300% while others

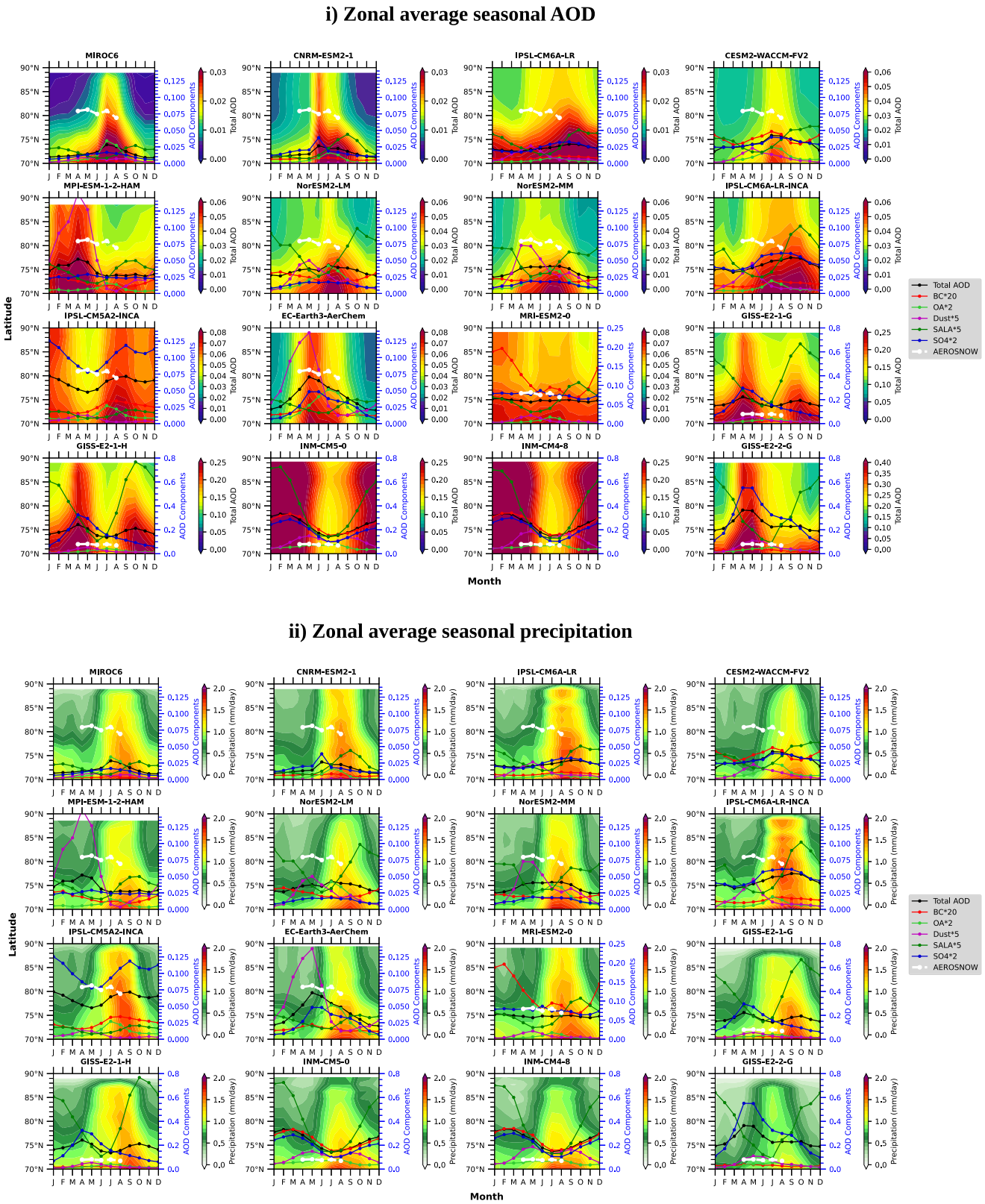

Fig. 6 | Zonal (latitude-month) averages of aerosol optical depth (AOD) and precipitation over Arctic sea-ice-covered regions (≥70°N) simulated by CMIP6 models. i shows total AOD (color shading) along with overlaid contributions from individual aerosol components (BC, OA, dust, sea salt, and sulfate; scaled as indicated) and AEROSNOW-derived AOD (white dashed line). **ii** shows total precipitation (color shading) for the same domain and period. Each subplot corresponds to a different model. The figure illustrates the seasonal and latitudinal evolution of aerosol loading and precipitation, highlighting inter-model differences in AOD magnitude, spatial distribution, and their relationship with precipitation intensity across the Arctic.

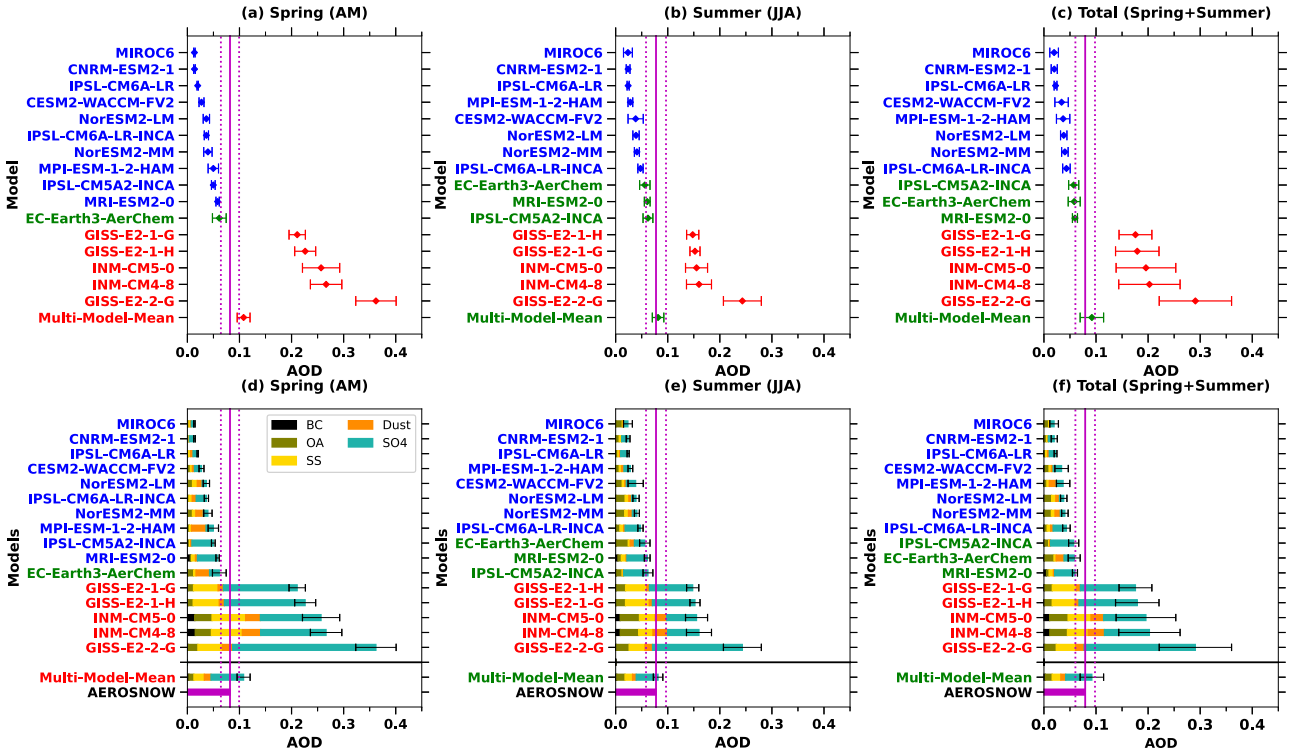

Fig. 7 | The seasonal mean AOD and its components are simulated by various numerical models. a–c Illustrate the seasonal averages for spring, summer, and their combined interval of AOD and its standard deviations for various models estimations, and AEROSNOW retrievals across the sea-ice area of the Arctic, respectively. **d–f** The panels display the average aerosol constituents for each model during spring, summer, and their combined period, alongside the ensemble mean and the corresponding AEROSNOW values for the high Arctic sea-ice domain. Models that yield total AOD lower than the AEROSNOW estimate are shown in blue, whereas those producing higher AOD values are indicated in red. The model simulations falling within two standard deviations are presented in green. Two-sigma limits are shown with dotted maroon lines, and the solid curves depict the AEROSNOW mean AOD.

nearly eliminate these components (Fig. S1). Such contrasting biases demonstrate that while the MMM appears close to observations in total AOD magnitude, it is not representative of actual aerosol composition or processes. The apparent match arises from error compensation—underestimation in some models offsetting overestimation in others—leading to misleading agreement with AEROSNOW data.

Because aerosol-cloud-climate interactions depend strongly on species composition, hygroscopicity, and size distribution, this error compensation in the MMM significantly distorts estimates of direct and indirect radiative forcing[12]. Over- or under-representation of scattering species (SO_4, SS) and absorbing components (BC) directly affects atmospheric heating rates, cloud albedo, and surface energy fluxes, thereby altering the simulated regional warming signal over Arctic sea ice. Consequently, reliance on the MMM for diagnosing aerosol-driven climatic impacts can obscure physically meaningful variability and lead to biased interpretations.

To address these limitations, we propose using the EC-Earth3-AerChem model for further investigation of aerosol processes and their impacts over the Arctic sea-ice region in a warming climate in scientific research. Among all CMIP6 models, EC-Earth3-AerChem demonstrates the closest agreement with AEROSNOW observations in both total AOD and the relative contributions of its aerosol components during spring and summer. The EC-Earth3-AerChem is well estimating the observed seasonal amplitude without introducing substantial biases in any aerosol type, indicating a well-balanced estimation of anthropogenic and natural processes associated with aerosols, long-range transport, wet scavenging, and secondary aerosols creation. Consequently, EC-Earth3-AerChem offers a physically consistent and observationally supported framework for exploring the seasonal influence of aerosols on regional radiative forcing and surface warming over the Arctic sea-ice domain (Figs. 4–6).

Discussion

Comparison between AEROSNOW observations and CMIP6 simulations reveals substantial discrepancies in both the magnitude and seasonal progression of AOD over Arctic sea-ice-covered regions (≥72°N). AEROSNOW shows spring (April–May) area-averaged AOD of ~0.08 ± 0.01, with localized maxima of 0.12–0.18 near marginal ice zones, decreasing to ~0.05–0.07 in summer (June–August). This reflects Arctic Haze conditions followed by cleaner summer conditions driven by enhanced wet scavenging and reduced transport[6]. In contrast, several models underestimate spring AOD (0.04–0.07), while others overestimate it (≥0.25). The multi-model mean (MMM) lies between these extremes and captures the general seasonal tendency, but this agreement results from compensating biases across models rather than a consistent representation of observed variability (Figs. 4–6).

These biases may reflect differences in the representation of aerosol emissions, transport, removal processes, and chemical processing across models; however, the present analysis does not allow for definitive attribution of the relative contributions of these processes. The low-AOD models (e.g., MIROC6, CNRM-ESM2-1, IPSL-CM6A-LR, CESM2-WACCM-FV2, MPI-ESM-1-2-HAM, NorESM2-LM, NorESM2-MM, IPSL-CM6A-LR-INCA, IPSL-CM5A2-INCA, and MRI-ESM2-0) simulate comparatively lower contributions of sulfate and black carbon to total AOD, whereas the high-AOD models (e.g., GISS-E2-1-G, GISS-E2-1-H, INM-CM5-0, INM-CM4-8, and GISS-E2-2-G) exhibit relatively larger contributions from sulfate and sea salt (Figs. 4 and 5). These differences represent inter-model variability in aerosol partitioning rather than observationally constrained biases. The resulting spread in species contributions contributes to differences in total AOD magnitude and seasonal evolution across models.

Among all models, EC-Earth3-AerChem exhibits the most realistic AOD seasonality, closely matching AEROSNOW observations in both

magnitude and timing (spring: 0.07–0.09; summer: 0.05–0.06). Its success arises from advanced parameterizations of atmospheric chemistry and meteorology, including interactive aerosol microphysics, detailed gas-phase and heterogeneous chemistry, and explicit, cloud-phase-dependent wet scavenging[30]. These schemes accurately simulate aerosol lifetimes, vertical distribution, and removal efficiency, while well-resolved meteorology enhances representation of transport and mixing. As a result, EC-Earth3-AerChem reproduces the observed transition from springtime Arctic Haze to summer clean-air conditions with minimal bias[30].

Given its good performance, the chemistry-meteorology coupling and wet scavenging parameterizations of EC-Earth3-AerChem[30] could serve as a benchmark for improving other CMIP6 models. Incorporating its interactive aerosol-chemistry module, physically based cloud microphysics, and precipitation-driven removal schemes could substantially reduce current inter-model spread and improve estimates of aerosol-cloud-radiation feedbacks. Such advancements are essential for refining projections of regional radiative forcing and sea-ice feedbacks in a warming Arctic.

Methods

Satellite measurements and retrieval framework

This work utilizes aerosol optical depth (AOD) observations retrieved from the Advanced Along-Track Scanning Radiometer (AATSR)[31] aboard the ENVISAT platform. AATSR was created by the European Space Agency's (ESA) long-term Earth observations, operating from 28 February 2002 until 8 April 2012 with a nominal equator crossing time of 10:00 local solar time. The instrument provides radiances at seven spectral channels spanning the visible to thermal infrared (0.55–12 μm), using a dual-view configuration that acquires a nadir measurement and a simultaneous forward-view observation at approximately 55°. This observational geometry, together with a nadir spatial resolution of ~1 km and a swath width of about 512 km, allows robust discrimination between atmospheric and surface contributions to the measured top-of-atmosphere (TOA) reflectance.

AOD retrievals for this study were produced using the AEROSNOW algorithm[25], a retrieval framework developed specifically for bright, cryospheric surfaces such as sea ice and snow. Traditional aerosol retrieval algorithms often fail at high latitudes because high surface reflectance and persistent cloudiness obscure aerosol signals. AEROSNOW circumvents these limitations by combining (i) physically based surface bidirectional reflectance distribution function (BRDF) parameterizations tailored for snow and sea ice, (ii) optimized Arctic cloud-masking procedures[27], and (iii) the multi-angle information content provided by AATSR's dual-view radiances. The algorithm retrieves AOD primarily at visible wavelengths (reference 550 nm), using a forward-model inversion that simultaneously constrains aerosol loading, surface reflectance, and viewing geometry effects. These features enable AEROSNOW to isolate aerosol-induced radiance perturbations even under conditions where traditional algorithms fail.

To assess the AEROSNOW retrievals, the dataset was evaluated against sun photometer measurements from several Arctic AERONET stations situated on snow- and ice-covered surfaces (including PEARL, OPAL, Hornsund, and Thule). Collocated comparisons show strong agreement, with a Pearson correlation coefficient of $R = 0.86$, low mean bias, and root-mean-square differences consistent with uncertainties expected for high-latitude optical retrievals. Importantly, retrieval errors remain small for AOD values below 0.15, a range typical of Arctic background aerosol conditions. These validation results, combined with the spatial and temporal coverage afforded by AATSR, establish AEROSNOW as a robust observational constraint for evaluating climate model simulations of aerosol seasonality over the Arctic sea-ice region.

Despite the good agreement with AERONET observations, uncertainties remain in the AEROSNOW retrievals due to the challenging radiative environment over Arctic snow and sea ice. The primary sources of uncertainty arise from (i) residual cloud contamination despite optimized cloud screening, (ii) uncertainties in the bidirectional reflectance distribution function (BRDF) parameterization used to represent highly reflective snow and ice surfaces, and (iii) reduced sensitivity of top-of-atmosphere reflectance to low aerosol loading under high surface albedo conditions. These factors can introduce both random retrieval noise and small systematic biases, particularly at very low AOD values. Based on the validation analysis presented in Swain et al.[25], the overall uncertainty of AEROSNOW AOD is comparable to typical satellite retrieval errors under bright surface conditions and remains within the range expected for high-latitude observations. In the context of this study, the magnitude of inter-model differences substantially exceeds the estimated retrieval uncertainty, supporting the suitability of AEROSNOW as an observational constraint for model evaluation.

The resulting dataset creates a unique, decade-long (2003–2011), high-resolution observational record of aerosol variability over Sea-ice areas of the Arctic. Its ability to resolve both spatial gradients (e.g., marginal ice zones) and temporal evolution (spring enhancement, summer minimum) makes it particularly valuable for assessing model performance in simulating Arctic aerosol regimes and for diagnosing deficiencies in aerosol transport, removal, and chemical processes.

Model data sets

The Model estimations used in this study were acquired from the Coupled Model Intercomparison Project Phase 6 (CMIP6)[32], which provides a coordinated ensemble of global numerical models (ESMs) and atmospheric chemistry-climate models designed to evaluate past and future estimations of climate change, including aerosol-radiation and aerosol-cloud interactions. CMIP6 models explicitly simulate key aerosol species—sulfate (SO_4), black carbon (BC), organic aerosol (OA), dust, and sea salt (SS)—along with their microphysical evolution, transport, and radiative impacts. These simulations offer an opportunity to examine how consistently modern climate models represent Arctic aerosol processes whose dynamics are tightly coupled to long-range transport, wet and dry deposition, and the seasonal variability of meteorology over sea ice.

For this analysis, sixteen different CMIP6 models were selected based on the availability of (i) monthly mean total AOD, (ii) speciated aerosol optical depth or mass fields (SO_4, BC, OA, SS, and dust), and (iii) complete temporal coverage for the period 2003–2011 to align with the AEROSNOW observational record. The selected models include MIROC6, CNRM-ESM2-1, IPSL-CM6A-LR, CESM2-WACCM-FV2, MPI-ESM-1-2-HAM, NorESM2-LM, NorESM2-MM, IPSL-CM6A-LR-INCA, IPSL-CM5A2-INCA, MRI-ESM2-0, EC-Earth3-AerChem, GISS-E2-1-G, GISS-E2-1-H, INM-CM5-0, INM-CM4-8, and GISS-E2-2-G. Detailed metadata—including model resolution, dynamical core, aerosol parameterization schemes, and the ensemble member used—are summarized in Table S1. All models were analyzed using their primary "historical" realizations, which are driven by the same prescribed emissions, ensuring consistent treatment of external forcings across the ensemble[32].

Each model incorporates its own aerosol microphysics and chemistry framework, which contributes to inter-model spread. For example, MPI-ESM-1-2-HAM includes the interactive Hamburg Aerosol Model (HAM), CESM2-WACCM employs a fully coupled chemistry-climate configuration with interactive stratospheric processes, while EC-Earth3-AerChem couples the TM5-based chemistry module with meteorology at high temporal frequency (Table S1). These structural differences influence aerosol life cycles—particularly long-range transport into the Arctic, scavenging by stratiform and convective precipitation, and the estimation of aerosols of natural origin, such as sea salt and biogenic aerosol emissions. Differences in radiative transfer schemes and aerosol optical property assumptions further influence model AOD fields and contribute to inter-model divergence.

To ensure a fair and consistent comparison with satellite observations, model AOD fields were pre-processed following standardized Arctic aerosol evaluation protocols[7,18,23]. Monthly AOD values were extracted from each model for grid cells corresponding to the Arctic sea-ice domain (≥72°N) and aligned with the temporal sampling of AEROSNOW. Specifically, AEROSNOW monthly averages were computed only when at least 15 days of valid

retrievals were available; the same temporal mask was applied to the model data to avoid sampling biases associated with cloud contamination or polar night conditions in the observations.

Spatial intercomparison between AEROSNOW and CMIP6 models required regridding all datasets to a common 1G × 1° latitude-longitude grid. Regridding was performed using the Climate Data Operators (CDO) tools[33], employing bilinear interpolation for intensive fields such as AOD. For models providing AOD at wavelengths other than 550 nm, spectral conversion was applied using Ångström exponents when available. All derived metrics—including absolute AOD differences, relative bias, seasonal means, and temporal variability—were calculated on this harmonized grid.

The MMM was then computed as the arithmetic average across the 16 regridded models for each grid cell and time step. While the MMM provides a useful ensemble benchmark, it may obscure compensating errors among models with strongly divergent AOD magnitudes. Therefore, individual model deviations were retained and analyzed throughout the study to diagnose structural and process-level inconsistencies in aerosol representation across the CMIP6 ensemble.

Data availability

Climate model outputs from CMIP6 are publicly available at https://esgf-node.llnl.gov/search/cmip6/. AATSR satellite data are available https://earth.esa.int/eogateway/instruments/aatsr/auxiliary-data. The AEROSNOW scheme methodology can be accessed at https://doi.org/10.5194/amt-17-359-2024.

Code availability

Code is available upon request to the corresponding author.

Received: 10 December 2025; Accepted: 19 April 2026;
Published online: 01 June 2026

References

1. Rantanen, M. et al. The arctic has warmed nearly four times faster than the globe since 1979. *Commun. Earth Environ.* **3**, 168 (2022).
2. Gillett, N. P. et al. Attribution of polar warming to human influence. *Nat. Geosci.* **1**, 750–754 (2008).
3. Swain, B. et al. Contrasting anthropogenic drivers behind asymmetric warming in the Arctic and Antarctica. *Ocean Land Atmos. Res.* **5**, 0127 (2026).
4. Rosenfeld, D. et al. Flood or drought: how do aerosols affect precipitation? *Science* **321**, 1309–1313 (2008).
5. Breider, T. J. et al. Multidecadal trends in aerosol radiative forcing over the Arctic: contribution of changes in anthropogenic aerosol to Arctic warming since 1980. *J. Geophys. Res. Atmos.* **122**, 3573–3594 (2017).
6. Willis, M. D., Leaitch, W. R. & Abbatt, J. P. Processes controlling the composition and abundance of arctic aerosol. *Rev. Geophys.* **56**, 621–671 (2018).
7. Swain, B. et al. Aerosols in the central arctic cryosphere: satellite and model integrated insights during arctic spring and summer. *Atmos. Chem. Phys.* **24**, 5671–5693 (2024).
8. Sand, M. et al. Aerosols at the poles: an aerocom phase II multi-model evaluation. *Atmos. Chem. Phys.* **17**, 12197–12218 (2017).
9. Swain, B. et al. Model simulations capture seasonal Arctic haze and clean-air cycle better than satellite and reanalysis. *Sci. Rep*. **15**, 42934 (2025).
10. Sand, M. et al. Aerosol absorption in global models from AerCom phase III. *Atmos. Chem. Phys.* **21**, 15929–15947 (2021).
11. Schmale, J., Zieger, P. & Ekman, A. M. Aerosols in current and future arctic climate. *Nat. Clim. Change* **11**, 95–105 (2021).
12. Schmale, J. et al. Pan-arctic seasonal cycles and long-term trends of aerosol properties from ten observatories. *Atmos. Chem. Phys. Discuss.* **2021**, 1–53 (2021).
13. Hoffmann, A. et al. Remote sensing and in-situ measurements of tropospheric aerosol, a pamarcmip case study. *Atmos. Environ.* **52**, 56–66 (2012).
14. Wendisch, M. et al. The Arctic Cloud Puzzle: using Cloud/Pascal multiplatform observations to unravel the role of clouds and aerosol particles in Arctic amplification. *Bull. Am. Meteorol. Soc.* **100**, 841 – 871 (2019).
15. Ohata, S. et al. Arctic black carbon during Pamarcmip 2018 and previous aircraft experiments in spring. *Atmos. Chem. Phys.* **21**, 15861–15881 (2021).
16. Shupe, M. D. et al. Overview of the MOSAiC expedition: atmosphere. *Elem. Sci. Anthr.* **10**, 00060 (2022).
17. Toth, T. D. et al. Minimum aerosol layer detection sensitivities and their subsequent impacts on aerosol optical thickness retrievals in CALIPSO level 2 data products. *Atmos. Meas. Tech.* **11**, 499–514 (2018).
18. Xian, P. et al. Arctic spring and summertime aerosol optical depth baseline from long-term observations and model reanalyses – part 2: statistics of extreme aod events, and implications for the impact of regional biomass burning processes. *Atmos. Chem. Phys.* **22**, 9949–9967 (2022).
19. Istomina, L. G., von Hoyningen-Huene, W., Kokhanovsky, A. A., Schultz, E. & Burrows, J. P. Remote sensing of aerosols over snow using infrared AATSR observations. *Atmos. Meas. Tech.* **4**, 1133–1145 (2011).
20. Mei, L. et al. Aerosol optical depth retrieval in the Arctic region using MODIS data over snow. *Remote Sens. Environ.* **128**, 234–245 (2013).
21. Mei, L. et al. On the retrieval of aerosol optical depth over cryosphere using passive remote sensing. *Remote Sens. Environ.* **241**, 111731 (2020).
22. Mei, L. et al. Retrieval of aerosol optical thickness in the Arctic snow-covered regions using passive remote sensing: impact of aerosol typing and surface reflection model. *IEEE Trans. Geosci. Remote Sens.* **58**, 5117–5131 (2020).
23. Xian, P. et al. Arctic spring and summertime aerosol optical depth baseline from long-term observations and model reanalyses–part 1: climatology and trend. *Atmos. Chem. Phys.* **22**, 9915–9947 (2022).
24. von Hardenberg, J. et al. Aerosol optical depth over the Arctic: a comparison of ECHAM-HAM and TM5 with ground-based, satellite and reanalysis data. *Atmos. Chem. Phys.* **12**, 6953–6967 (2012).
25. Swain, B. et al. Retrieval of aerosol optical depth over the Arctic cryosphere during spring and summer using satellite observations. *Atmos. Meas. Tech.* **17**, 359–375 (2024).
26. Kokhanovsky, A. A. & Breon, F.-M. Validation of an analytical snow BRDF model using Parasol multi-angular and multispectral observations. *IEEE Geosci. Remote Sens. Lett.* **9**, 928–932 (2012).
27. Jafariserajehlou, S. et al. A cloud identification algorithm over the arctic for use with aatsr–slstr measurements. *Atmos. Meas. Tech.* **12**, 1059–1076 (2019).
28. Ren, L. et al. Source attribution of arctic black carbon and sulfate aerosols and associated arctic surface warming during 1980–2018. *Atmos. Chem. Phys.* **20**, 9067–9085 (2020).
29. Swain, B. et al. Insights of aerosol-precipitation nexus in the central Arctic through CMIP6 climate models. *npj Clim. Atmos. Sci.* **8**, 103 (2025).
30. Van Noije, T. et al. Ec-earth3-aerchem, a global climate model with interactive aerosols and atmospheric chemistry participating in CMIP6. *Geosci. Model Dev. Discuss.* **2020**, 1–46 (2020).
31. Jones, D. L. & Remedios, J. The advanced along track scanning radiometer (AATSR) and its predecessors ATSR-1 and ATSR-2: an introduction to the special issue. *Remote Sens. Environ*. **116**, 1–3 (2012).
32. Eyring, V. et al. Overview of the coupled model intercomparison project phase 6 (cmip6) experimental design and organization. *Geosci. Model Dev.* **9**, 1937–1958 (2016).
33. Schulzweida, U., Kornblueh, L. & Quast, R. CDO User Guide (Version 1.9.8). Max Planck Institute for Meteorology. https://code.mpimet.mpg.de/projects/cdo/embedded/cdo.pdf (2019).

Acknowledgements
We express gratitude to the CMIP6 model community for sharing their data and to ESA for providing the AATSR dataset. This research has received funding from the University and the state of Bremen by Dr. Marco Vountas, as well as from the Deutsche Forschungsgemeinschaft (DFG, German Research Foundation) under the project 'ArctiC Amplification: Climate Relevant Atmospheric and SurfaCe Processes, and Feedback Mechanisms (AC)3' as part of the Transregional Collaborative Research Center (TRR) 172, Project-ID 268020496.

Author contributions
B.S. conceived and designed the research undertaken in this study. B.S. analyzed the datasets and generated the plots. All the co-authors, M.V., A.S., L.A., I.T., L.L., R.S., B.H., N.M., and H.B. helped in shaping the manuscript. All authors contributed to the interpretation of the results and the preparation of the final manuscript.

Funding
Open Access funding enabled and organized by Projekt DEAL.

Competing interests
The authors declare no competing interests.

Additional information
Supplementary information The online version contains supplementary material available at https://doi.org/10.1038/s44407-026-00080-7.

Correspondence and requests for materials should be addressed to Basudev Swain or Marco Vountas.